1 **Building a machine learning surrogate model for wildfire activities within a global earth**
2 **system model**

3 Qing Zhu[1,*], Fa Li[1,2], William J. Riley[1], Li Xu[3], Lei Zhao[4], Kunxiaojia Yuan[1,2], Huayi Wu[2],
4 Jianya Gong[5], James Randerson[3]
5
6 [1] Climate and Ecosystem Sciences Division, Climate Sciences Department, Lawrence Berkeley
7 National Laboratory, Berkeley, CA, USA
8 [2] State Key Laboratory of Information Engineering in Surveying, Mapping and Remote Sensing,
9 Wuhan University, Wuhan, China
10 [3] Department of Earth System Science, University of California Irvine, Irvine, CA, USA
11 [4] Department of Civil and Environmental Engineering, University of Illinois Urbana-Champaign,
12 Champaign, IL, USA
13 [5] School of Remote Sensing and Information Engineering, Wuhan University, Wuhan, China
14 *Correspondence to Qing Zhu (qzhu@lbl.gov)

15   **Abstract**

16   Wildfire is an important ecosystem process, influencing land biogeophysical and

17   biogeochemical dynamics and atmospheric composition. Fire-driven loss of vegetation cover, for

18   example, directly modifies the surface energy budget as a consequence of changing albedo,

19   surface roughness, and partitioning of sensible and latent heat fluxes. Carbon dioxide and

20   methane emitted by fires contribute to a positive atmospheric forcing, whereas emissions of

21   carbonaceous aerosols may contribute to surface cooling. Process-based modeling of wildfires in

22   earth system land models is challenging due to limited understanding of human, climate, and

23   ecosystem controls on fire number, fire size, and burned area. Integration of mechanistic wildfire

24   models within Earth system models requires careful parameter calibration, which is

25   computationally expensive and subject to equifinality. To explore alternative approaches, we

26   present a deep neural network (DNN) scheme that surrogates the process-based wildfire model

27   with the Energy Exascale Earth System Model (E3SM) interface. The DNN wildfire model

28   accurately simulates observed burned area with over 90% higher accuracy with a large reduction

29   in parameterization time compared with the current process-based wildfire model. The surrogate

30   wildfire model successfully captured the observed monthly regional burned area during

31   validation period 2011 to 2015 (coefficient of determination, $R^2 = 0.93$). Since the DNN wildfire

32   model has the same input and output requirements as the E3SM process-based wildfire model,

33   our results demonstrate the applicability of machine learning for high accuracy and efficient

34   large-scale land model development and predictions.

1. Introduction

Wildfires burn ~500 million hectares of vegetated land surface each year, which significantly modifies the physical properties and biogeochemical cycles of terrestrial ecosystems [*Andela et al.*, 2017; *Bond-Lamberty et al.*, 2007; *Pellegrini et al.*, 2018; *Randerson et al.*, 2006]. Living vegetation biomass, surface litter, and coarse woody debris are directly combusted and removed by wildfire [*Harden et al.*, 2006; *Walker et al.*, 2019]. It has been suggested that global forest would double if fire were eliminated [*Bond et al.*, 2005]. Fire has multiple important consequences for the climate system, including directly releasing greenhouse gases (*e.g.*, CO_2, CH_4) [*Kasischke and Bruhwiler*, 2002; *Ross et al.*, 2013] and aerosols [*Jiang et al.*, 2020]; changing land surface albedo and energy budgets [*French et al.*, 2016; *Rother and De Sales*, 2020] and land-atmosphere exchanges of heat, mass, and momentum [*Chambers and Chapin*, 2002]; limiting plant transpiration and regional water recycling [*Brando et al.*, 2020; *Holden et al.*, 2018]; and reshaping forest composition [*Mekonnen et al.*, 2019]. In addition, biomass burning emits a large amount of fine particulate matter that contributes to about 30% of cloud condensation nuclei globally [*Day*, 2004]. Soil organic matter decomposition, nitrogen mineralization, and the richness and diversity of soil fungal communities [*Oliver et al.*, 2015] could also be influenced by wildfire through modifying litter substrate supply and degraded enzymatic activities [*Bowd et al.*, 2019; *Holden et al.*, 2018; *Pellegrini et al.*, 2018; *Pellegrini et al.*, 2020].

Climate change and land use activities have jointly affected fire spatial distribution, frequency, and intensity [*Andela et al.*, 2017; *Kelley et al.*, 2019; *X Xu et al.*, 2020] since the pre-industrial era. For example, warmer and drier climate conditions enhance fuel aridity and favor fire occurrence in forest ecosystems where fuels have built up over a period of decades and centuries [*Abatzoglou and Williams*, 2016; *Williams et al.*, 2019]. Even if annual precipitation does not decline, redistribution of precipitation towards wet season extreme rainfall events could contribute to longer dry periods and thus more severe fire activity [*X Xu et al.*, 2020]. Human activities often shape wildfire activity through regulating patterns of ignition and fire occurrence (*e.g.*, powerline ignition) [*Keeley and Syphard*, 2018] and suppressing wildfire activity by means of land fragmentation, fire management, and livestock grazing [*Andela et al.*, 2017]. In California, fire density is highly associated with population density and the distance to the wildland urban interface (WUI) [*Syphard et al.*, 2007]. At the global scale, along gradients of

66   increasing population density, fire frequency initially increases by up to 20% and then gradually

67   declines in more densely populated areas [*Knorr et al.*, 2014].

68   Although global wildfire burned area has declined over the recent two decades [*Andela et

69   al.*, 2017], many vulnerable ecosystems and geographic regions have experienced significant

70   increases in wildfire activity [*Abatzoglou and Williams*, 2016; *Walker et al.*, 2019] resulting in

71   large losses of natural resources and economic assets [*Papakosta et al.*, 2017; *Stephenson et al.*,

72   2013]. Over western U.S. forests, wildfire has dramatically increased, costing billions of dollars

73   each year and gaining wide public attention. This regional wildfire increase is mainly driven by

74   concurrent increases of spring temperature and declining snowpack [*Westerling et al.*, 2006],

75   mid-summer increases in vapor pressure deficit [*Williams et al.*, 2019], and increases in drought

76   stress during fall [*Goss et al.*, 2020]. The enhancement of wet and dry oscillations favors initial

77   vegetation growth and subsequent wildfire activity [*Heyerdahl et al.*, 2002; *Saha et al.*, 2019].

78   Wildfire models have played an important role in many aspects of wildfire research,

79   including monitoring fire spread [*Finney*, 1998; *Radke et al.*, 2019], analyzing controllers of

80   wildfire short-term and long-term variability [*Kelley et al.*, 2019], predicting severity of the

81   upcoming fire seasons [*Preisler and Westerling*, 2007] and climate-scale fire variability

82   [*Girardin and Mudelsee*, 2008; *Yue et al.*, 2013], and understanding the complex climate-

83   wildfire-ecosystem feedbacks [*Clark et al.*, 2004; *Mekonnen et al.*, 2019; *Zou et al.*, 2020]. Two

84   types of wildfire models are widely used: process-based models and data-driven statistical

85   models [*Hantson et al.*, 2016]. Process-based wildfire models consider detail processes related to

86   natural fire ignition [*Prentice and Mackerras*, 1977], anthropogenic ignition [*Venevsky et al.*,

87   2002], fire spread and duration [*Thonicke et al.*, 2010], fire suppression [*Lenihan and Bachelet*,

88   2015], and fire mass and heat fluxes [*F Li et al.*, 2012]. Process-based wildfire models have been

89   widely used in dynamic vegetation models and coupled earth system models (ESMs) with

90   various complexities of parameterization [*Fang Li et al.*, 2019; *Rabin et al.*, 2017]. As more and

91   more detailed fire processes are considered and parameterized, structural and parametric

92   uncertainties may increase due to incomplete representation of individual processes and

93   imperfect mathematical formulation [*Riley and Thompson*, 2017]. Historically, data-driven

94   models were often used for fire behavior modeling and aim to track the ignition, spread,

95   duration, and extinction of individual fires [*Finney*, 1998; *Radke et al.*, 2019] at fine spatial and

96   temporal scales. This group of models are more relevant to operational fire research. While

97   process-based wildfire models in the context of global vegetation models or earth system land

98   models focuses on the gridcell aggregated fire burned area dynamics that are more relevant to

99   researches on large scale patterns and climate scale predictions [*Fang Li et al.*, 2019; *Rabin et*

100   *al.*, 2017]. This study particularly focuses on the second category of wildfire models.

101   Although explicit processes are simulated, the accuracy of process-based wildfire models

102   are highly dependent on parameterization, which is computationally expensive [*Teckentrup et*

103   *al.*, 2018; *L Xu et al.*, 2021; *Zhu and Zhuang*, 2014]. Data-driven models, however, directly link

104   the driving variables (*e.g.*, climate factors) to the fire activity using simple statistical models or

105   more sophisticated machine learning techniques, ignoring the explicit processes and feedbacks

106   associated with wildfire [*Ganapathi Subramanian and Crowley*, 2018; *Radke et al.*, 2019; *Tonini*

107   *et al.*, 2020]. Through training and validation, statistical representations of wildfire dynamics are

108   learned by models using principles from machine learning. Data-driven wildfire models are

109   diverse in terms of driving variables and model structure. For example, many current machine

110   learning wildfire models rely on remote oceanic dynamics (*e.g.*, sea surface temperature

111   variability) and atmospheric teleconnections to simulate land surface fire activities [*Chen et al.*,

112   2020; *Chen et al.*, 2011; *Yu et al.*, 2020]. Another group of data-driven wildfire models draws

113   more heavily upon regional climate, plant functional type, and human infrastructure driver

114   variables [*Coffield et al.*, 2019; *Sayad et al.*, 2019].

115   In this study, we develop a machine learning wildfire model using the process

116   representation of wildfire in the Energy Exascale Earth System Model (E3SM) land model

117   (ELMv1) [*Zhu et al.*, 2019], five observationally inferred burned area products [*Andela et al.*,

118   2019; *Giglio et al.*, 2018; *Lizundia-Loiola et al.*, 2020; *Lizundia-Loiola et al.*, 2018; *Van Der*

119   *Werf et al.*, 2017], and a deep neural network approach [*Goodfellow et al.*, 2016]. We

120   implemented a deep learning model that can better capture the complex and non-linear

121   interactions between controlling factors and wildfire activity. The objectives of this study are to

122   surrogate the wildfire parameterization in ELMv1 with the deep neural network and improve the

123   model simulated wildfire burned area across various fire regions [*Giglio et al.*, 2013].

124

125   **2. Methodology**

126   **2.1 ELMv1 wildfire model**

127   The process-based wildfire model in ELMv1 originates from the Community Land

128   Model (CLM4.5) [*F Li et al.*, 2012]; we take this wildfire model as the baseline (hereafter refer

129   to as BASE-Fire) without modification on process representation. BASE-Fire combines

130   information regarding ignition, fuel conditions, surface climate, and anthropogenic suppression

131   to simulate total burned area based on the fire counts and spread area of each fire (Figure 1). The

132   fire count in BASE-Fire is modeled as the sum of anthropogenic ignition and natural ignition,

133   where the latter is proportional to lightning density [*Prentice and Mackerras*, 1977] and the

134   former is determined by population density [*Venevsky et al.*, 2002]. Human activity may also

135   intentionally suppress wildfire occurrence if the fire is detected at early stage. For example,

136   developed regions with high population density and gross domestic product are less likely to use

137   fire to remove surface biomass. On the other hand, developed regions more likely suppress fire

138   given more effective fire management policy and suppression capability. Fire count is also

139   affected by surface fuel availability (aboveground biomass) and fuel combustibility (relative

140   humidity, topsoil temperature and moisture). The fire spread area in BASE-Fire is modeled as an

141   elliptical shaped region controlled by wind speed and fuel wetness [*Rothermel*, 1972] (using

142   topsoil (0 – 15 cm) moisture as a proxy). The fire duration is set to be one day based on a study

143   that reported years 2001-2004 mean global fire persistence [*Giglio et al.*, 2006a]. BASE-Fire

144   also does not explicitly consider roads, rivers, and firefighting activity [*Arora and Boer*, 2005].

145

146
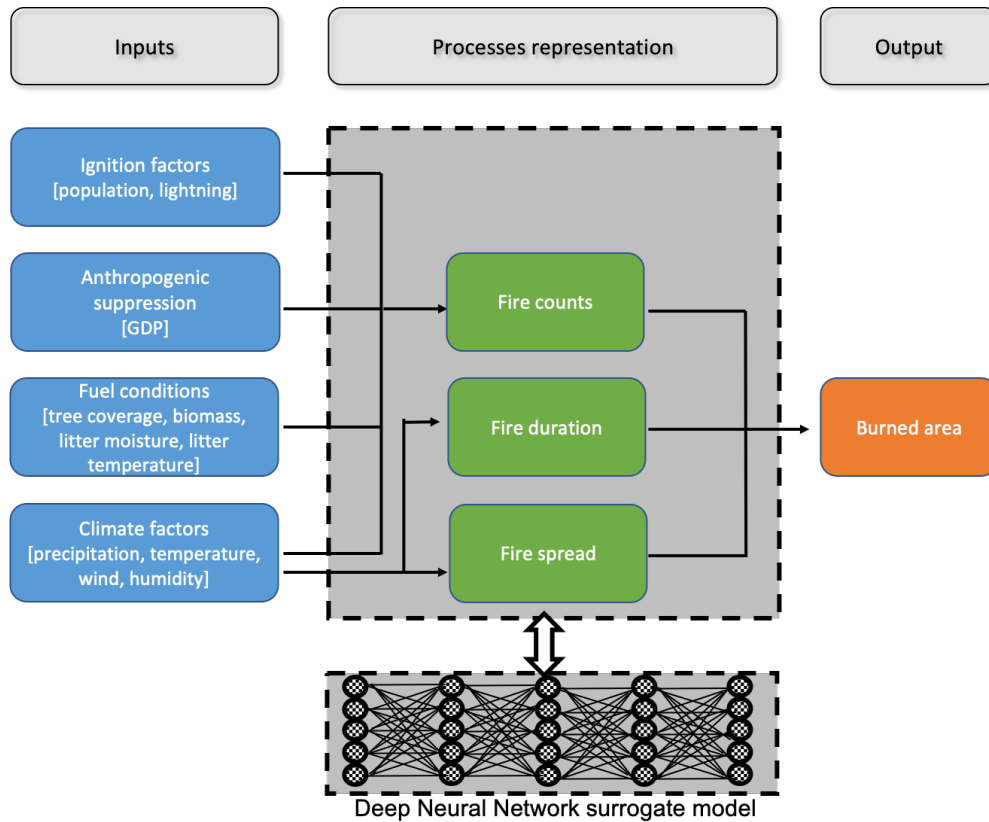
Figure 1. Schematic representation of the ELMv1 process-based BASE-Fire model and the
components to be surrogated with the Deep Neural Network (DNN) model (dark grey).

2.2 Deep neural network wildfire surrogate model

We developed the new fire model in two steps: (1) surrogating BASE-Fire with a deep
neural network (DNN) approach and (2) improving that surrogate model using five
observationally inferred burned area products (Table S1). First, we surrogated BASE-Fire with a
DNN approach (hereafter refer to as DNN-Fire) that uses the same input and output variables as
BASE-Fire but treats the explicit intermediate processes (*e.g.*, ignition, fire spread) as latent
variables coded by hidden layers in the DNN (Figure 1). DNN-Fire was developed with five
hidden layers and five neurons in each layer for burned area simulation. The DNN approach uses
a fully-connected feedforward neural network [*Schmidhuber*, 2015] that comprises input, hidden,
and output layers:

$$h_1 = f_1(W_1 I + b_1) \quad (1)$$
$$h_2 = f_2(W_2 h_1 + b_2) \quad (2)$$

$$h_3 = f_3(W_3h_2 + b_3) \quad (3)$$
$$h_4 = f_4(W_4h_3 + b_4) \quad (4)$$
$$h_5 = f_5(W_5h_4 + b_5) \quad (5)$$
$$O = f_6(W_6h_5 + b_6) \quad (6)$$

160   where I denotes the input layer (*e.g.*, climate factors) with 11 neurons, each corresponding to an

161   input variable listed in Table 1. h_1, h_2, h_3, h_4, and h_5 are five hidden vectors that are calculated

162   with two steps. First is a linear combination of previous layers' input vector (h) and the trainable

163   weight parameter matrix [W_1, W_2, W_3, W_4, W_5, W_6], considering biases b_1, b_2, b_3, b_4, b_5, and b_6.

164   Then, nonlinear activation functions f_1, f_2, f_3, f_4, f_5, and f_6. are applied to the output from the

165   previous step. In this study we used *softplus* as the activation function [*Zheng et al.*, 2015] that is

166   a non-linear transformation of input signals. O denotes the output layer that summarize the latent

167   variables from the last hidden layer (h_5) and calculate burned area.

168   **Table 1.** Input and output variables of ELMv1 BASE-Fire and surrogate DNN-Fire models

Variable category	Variable name	Data source and reference
Input variables		
Fuel conditions	Tree coverage	LUH2 [*Hurtt et al.*, 2020]
	Fuel load	ELMv1 total biomass [*Zhu and Riley*, 2015; *Zhu et al.*, 2019]
	Fuel wetness	ELMv1 topsoil moisture [*Zhu and Riley*, 2015; *Zhu et al.*, 2019]
	Fuel temperature	ELMv1 topsoil temperature [*Zhu and Riley*, 2015; *Zhu et al.*, 2019]
Climate factors	Precipitation	GSWP3 [*Dirmeyer et al.*, 2006]
	Near surface temperature	GSWP3 [*Dirmeyer et al.*, 2006]
	Wind speed	GSWP3 [*Dirmeyer et al.*, 2006]
	Relative humidity	GSWP3 [*Dirmeyer et al.*, 2006]
Ignition	Population density	[*Dobson et al.*, 2000]
	Lightning frequency	NASA-LIS/OTD [*Cecil et al.*, 2014]
Anthropogenic suppression	GDP	[*van Vuuren et al.*, 2007]
	Population density	[*Dobson et al.*, 2000]

	output variable
Burned area	ELMv1 percentage burned area [*Zhu and Riley*, 2015; *Zhu et al.*, 2019]

169

170   Second, we improved the surrogate DNN-Fire by fine-tuning the weight parameters using

171   observations (hereafter refer to DNN-Fire-OBS). Between 2001 and 2010, we initialized

172   DNN-Fire-OBS's weight parameters (W_1, W_2, W_3, W_4, W_5, and W_6) using results from DNN-Fire,

173   replaced the BASE-Fire burned area by the ensemble mean of five observationally inferred

174   burned area products including GFEDv4s [*Van Der Werf et al.*, 2017], Fire_CCI51 [*Lizundia-*

175   *Loiola et al.*, 2020], Fire_CCILT11 [*Lizundia-Loiola et al.*, 2018], MODIS MCD64 [*Giglio et*

176   *al.*, 2018], and Fire_Atlas [*Andela et al.*, 2019] (Table S1), and adjusted weight parameters until

177   the model best reproduced the observed burned area. This two-step approach will also allow

178   rapid parameterization of the Fire model as new fire data and baseline fire model results become

179   available. DNN-Fire-OBS can be more easily generalized since BASE-Fire provides explicit

180   physical guidance and a larger-than-observation input and output feature space for development

181   of the machine learning fire model. One limitation is the large discrepancy among five burned

182   area products. Tuning DNN-Fire towards the ensemble mean of the five products will potentially

183   compromise the data difference, however, future work is needed to improve the burned area data

184   quality and consistency.

185   **2.3 Model setup and simulation protocol**

186   We ran ELMv1 with BASE-Fire at 1.9° by 2.5° spatial resolution [*Zhu et al.*, 2020; *Zhu*

187   *et al.*, 2016] to generate training and testing datasets for the DNN wildfire model. BASE-Fire

188   was first spun up for 600 years with accelerated soil decomposition followed by 200 years

189   regular spinup with regular soil decomposition [*Koven et al.*, 2013]. The spinup simulations were

190   forced with constant atmospheric CO_2 concentration (285 ppmv) and 1901-1920 repeated

191   climate forcing from GSWP3 (Global Soil Wetness Project) [*Dirmeyer et al.*, 2006]. The purpose

192   of the spinup was to initialize ecosystem carbon pools and stabilize plant and soil carbon and

193   water fluxes. Restarting from the "spunup" conditions, a transient simulation was then conducted

194   from 1901 to 2015 with GSWP3 transient climate forcing, atmospheric CO_2 concentrations, and

195   nitrogen and phosphorus deposition [*Lamarque et al.*, 2005; *Mahowald et al.*, 2008]. Wildfire

196   associated variables were selected for output with a monthly temporal resolution (Table 1).

197   BASE-Fire output from years 1981 to 2010 were used to train, test, and fine-tune

198   DNN-Fire. We developed 14 region-specific models, corresponding to 14 widely used GFED

199   regions. For each region, all land gridcells (comprising no fire history, infrequent fire, and

200   repeated fire) were concatenated into one data matrix (where rows consist of the number of

201   samples and columns of the number of variables). 80% of the data matrix was randomly sampled

202   for the training dataset and the remaining 20% of the data were reserved for testing. Furthermore,

203   the random sampling was stratified in order to reduce the risk of sampling, e.g., adjacent high

204   fire grid cells. All grid cells were first divided into three "strata": low burn (0-33% percentile),

205   median burn (33%-66% percentile), and high burn (67-100% percentile) grid cells based on the

206   magnitude of the burn. The stratified random sample assured the sampled grid cells for training

207   and testing had the same ratios of low/medium/high burn, thus eliminating the sampling bias

208   from spatial autocorrelation [*Wang et al.*, 2012]. In addition to random sampling, we also

209   investigated the impacts of data choice on the model performance, by sampling the testing

210   datasets within specific years (*e.g.*, 2001-2002, 2003-2004, 2005-2006, 2007-2008, 2009-2010)

211   and used the rest of the years for training. We found neglected differences among the models

212   (Figure S1) indicating the choice of training/testing data years were not impactful. Therefore, we

213   will discuss the results with stratified random sampling approach as the major results throughout

214   the paper.

215   All training and testing datasets were normalized to the range [0, 1] with the following

216   scaler:

$$X = \frac{\text{X} - X_{min}}{X_{max} - X_{min}} \qquad (7)$$

217   where *X* is the variable vector of interest and X_{min} and X_{max} are minimum and maximum values of

218   *X*, respectively. During the training stage, we randomly initialized the weighting parameters (Eq.

219   1-6) and optimized them using the Adaptive Moment Estimation method [*Kingma and Ba*,

220   2014], which is a variant of the gradient descent optimization method but considers adaptive

221   learning rate and momentum-like exponentially decaying gradients. The parameter optimization

222   aimed to minimize a mean squared error cost function:

$$J = \frac{1}{n}\sum_{i=1}^{n}(y_i^{DNN} - y_i^{BASE})^2 \qquad (8)$$

223   where y_i^{DNN} and y_i^{BASE} are DNN-Fire and BASE-Fire generated burned area, respectively. *i*

224   represents different gridcell. Cost function *J* summarizes the overall magnitude of the error

225 between the surrogate DNN-Fire and BASE-Fire. We then evaluated model performance using

226 metrics of mean absolute error (Eqn. 9), Pearson correlation (Eqn. 10), and coefficient of

227 determination (Eqn. 11).

228 $$MAE = \frac{1}{n}\sum_{i=1}^{n}|y_i^{DNN} - y_i^{BASE}| \qquad (9)$$

229 $$p = \frac{covariance(y^{DNN}, y^{BASE})}{variance(y^{DNN})variance(y^{BASE})} \qquad (10)$$

230 $$R^2 = 1 - \frac{\sum_{i=1}^{n}(y_i^{DNN} - y_i^{BASE})^2}{\sum_{i=1}^{n}(y_i^{BASE} - y_{mean}^{BASE})^2} \qquad (11)$$

231

232 **3. Results and discussion**

233 **3.1 Evaluation of wildfire surrogate model**

234   BASE-Fire performed reasonably well for total global burned area (508 ± 53 Mha yr^{-1}

235 (million hector per year) between years 2001 and 2010 compared with the observational long-

236 term average of 424~484 Mha yr^{-1}; Figure 2, Table S1). BASE-Fire also captured the global

237 declining trend of wildfire burned area over this time period, attributed to a decrease in tropical

238 fires [*Andela et al.*, 2017]. At the regional scale, however, BASE-Fire underestimated tropical

239 (S23.5° - N23.5°) burned area and overestimated temperate (N23.5° - N67.5°) and boreal (N67.5

240 above) burned area (Figure 2). Large spatial heterogeneity existed for BASE-Fire regional bias.

241 For example, over tropical GFED regions, BASE-Fire overestimated wildfire burned area over

242 Southern Hemisphere South America (SHSA), but underestimated wildfire burned area over both

243 Southern and Northern Hemisphere Africa regions (SHAF and NHAF), despite an overall

244 underestimation over the tropical region (Figure 3). In contrast, consistent overestimation

245 occurred over all temperate GFED regions. For example, wildfire burned was overestimated by

246 about a factor of 16 (~1 versus 16 Mha yr^{-1}) over the Europe GFED region (EURO) (Figure 3).

247 Although there is room to improve BASE-Fire performance, the parameterization would involve

248 large ensemble simulations and computational resources. Instead, we first used BASE-Fire

249 generated data as training and testing datasets to parameterize DNN-Fire, then we fine-tuned the

250 DNN-Fire model against observed burned area.

251
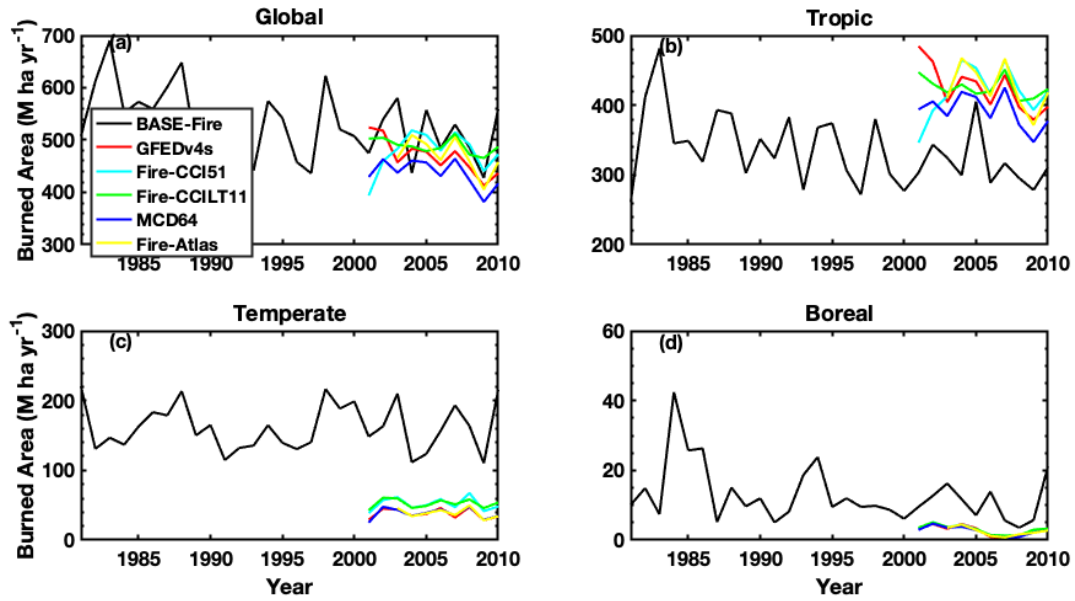
Figure 2. ELMv1 process-based model (BASE-Fire) simulated and five observationally inferred burned area products (Table S1) at (a) global scale; (b) Tropical (S23.5° -N23.5°); (c) Temperate (N23.5° - N 67.5°); and (d) Boreal (north of N 67.5°) regions.

255

256
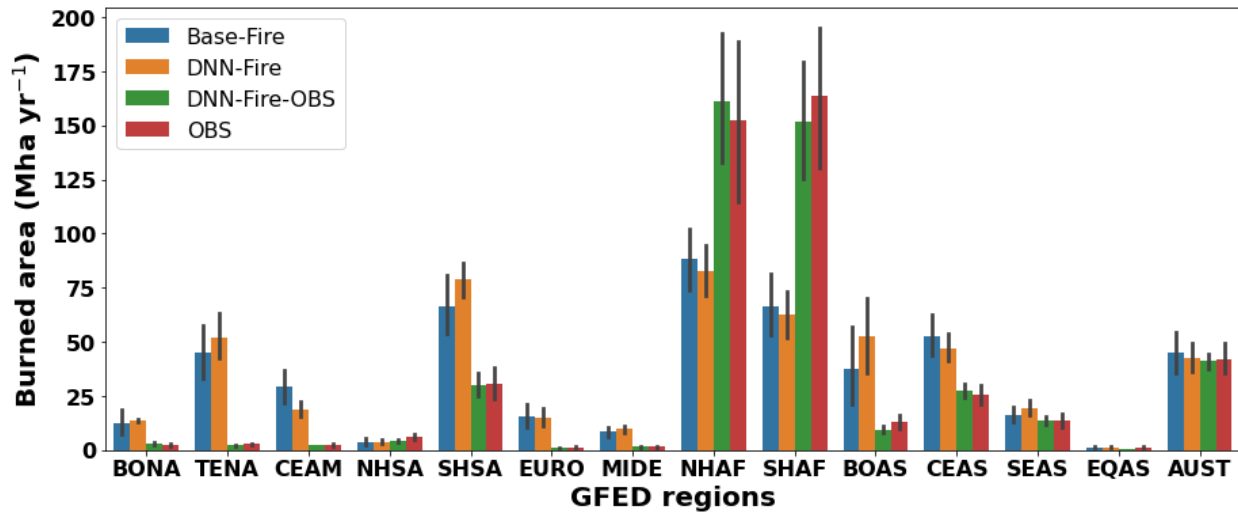
Figure 3. A comparison of wildfire burned area between estimates from the ELMv1 process-based model (BASE-Fire), Deep Neural Network wildfire model (DNN-Fire), Deep Neural Network wildfire model fine-tuned with observed burned area (DNN-Fire-OBS), and observations over 14 GFED fire regions.

261

262   Next we parameterized and compared DNN-Fire with BASE-Fire outputs. Using BASE-

263   Fire generated 1.9° × 2.5° resolution datasets of surface fuel conditions (fuel load (vegetation

264   biomass), fuel temperature (topsoil temperature), and fuel wetness (topsoil moisture)) with

265   gridded climate forcing (GSWP3) [*Dirmeyer et al.*, 2006], land use (LUH2 dataset) [*Hurtt et al.*,

266   2020], and social economic [*Dobson et al.*, 2000; *van Vuuren et al.*, 2007] factors, DNN-Fire

267   captured the spatial pattern of BASE-fire predicted wildfire activity (Figure 4, Figure S2).

268   Across all GFED regions, mean absolute error of DNN-Fire was 4.4 Mha yr^{-1} (<1% of total burn

269   area), with median and maximum errors of 1.8 and 13.0 Mha yr^{-1}, respectively (Figure 3).

270   Equatorial Asia (EQAS), Northern Hemisphere South America (NHSA), Central America

271   (CEAS), and Europe (EURO) regions had the lowest DNN-Fire errors (< 1.0 Mha yr^{-1}), while

272   Southern Hemisphere Africa (SHAF), and Boreal Asia (BOAS) had the largest errors (10-13

273   Mha yr^{-1}). Overall, the correlation coefficient between BASE-Fire and DNN-Fire simulated

274   burned area was 0.91 (*p* value < 0.01) and the coefficient of determination (R^2) was 0.79. Across

275   seasons, DNN-Fire also reasonably captured the BASE-Fire peak fire months (June to October),

276   which were dominated by Southern Hemisphere Africa and Southern Hemisphere South

277   America (Figure 5).

278   By surrogating BASE-Fire, DNN-Fire is expected to have similar biases and

279   uncertainties. The deficiency of BASE-Fire model will propagate to DNN-Fire. In our future

280   work we will overcome such limitation by training multiple DNN-Fire models with ensemble

281   simulations of BASE-Fire models that differ in critical parameters and vary in model structures.

282

283
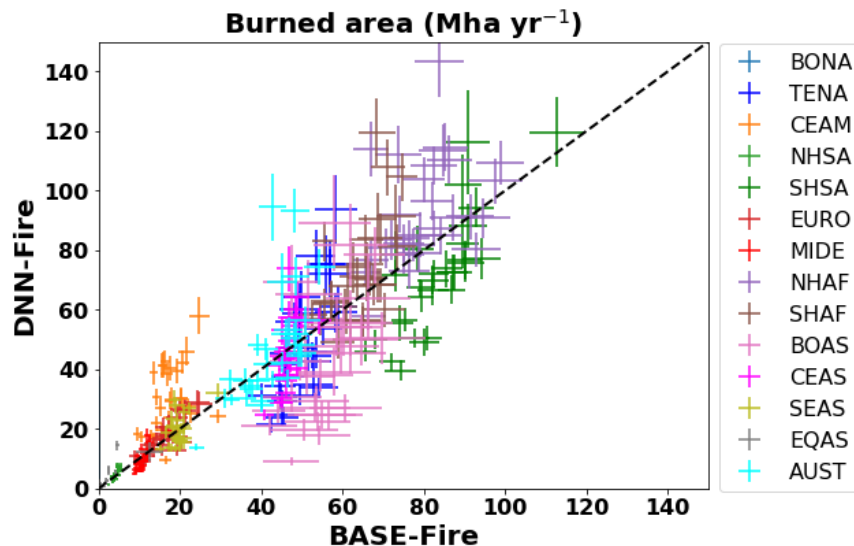
Figure 4. The performance of the Deep Neural Network wildfire model (DNN-Fire), compared with the original ELMv1 process-based wildfire model (BASE-Fire) over 14 GFED regions between years 2001 and 2010.

3.2 Calibrating the wildfire surrogate model using observations

Although the global pattern was reasonably captured, BASE-Fire had relatively large biases in several GFED regions, as discussed above. Since DNN-Fire was trained and validated only with BASE-Fire generated inputs (*e.g.*, fuel conditions) and outputs (burned area), we expect that, at best, DNN-Fire would have comparable biases as BASE-Fire. Starting from DNN-Fire, we further calibrated the model weighting parameters to create DNN-Fire-OBS and validated DNN-Fire-OBS performance using observed burned area from five existing burned area products (Table S1) between years 2001 and 2010. The calibration time cost several minutes with Intel Xeon Phi Processor 7250 processor.

Dramatic improvements were found in most of the 14 regions simulated by DNN-Fire-OBS (Figure 3). Overall, DNN-Fire-OBS simulated global long-term average burned area was 458 Mha yr^{-1} (compared with observational average 467 Mha yr^{-1}). Averaged across 14 regions, 73% reduction of mean absolute error was achieved by DNN-Fire-OBS, compared with the BASE-Fire model. Pearson correlation coefficient between the DNN-Fire-OBS simulated and observational burned area was 0.98 (*p* value < 0.001) with an R^2 of 0.97. Bias reduction was disproportionally distributed across the GFED regions (Figure 3). For example, severely burned regions, including Southern and Northern Hemisphere Africa (SHAF and NHAF) and Southern Hemisphere South America (SHSA) greatly benefited from the tuning and their regional biases were reduced by 88, 65, and 51 Mha yr^{-1} (or 88%, 89%, 98% reduction), respectively. Although Temperate Northern America (TENA) and Europe (EURO) wildfire burned area is relatively small (1-3 Mha yr^{-1}), the impacts of wildfire activity were significant due to their high population densities. DNN-Fire tended to overestimate the burned area in TENA and EURO by 47 and 13 Mha yr^{-1}, while DNN-Fire-OBS significantly reduced biases in both regions to less than 0.3 Mha yr^{-1} (a 97-98%% reduction).

BASE-Fire tended to overestimate inter-annual variability (IAV) and had opposite burned area anomalies between years 2001 and 2005. DNN-Fire dampened BASE-Fire's IAV, but had systematic overestimation of burned area. DNN-Fire-OBS agreed well with the observed IAV

315 between years 2001 and 2010 (Figure 5a). The seasonal cycle was also improved in DNN-Fire-

316 OBS in terms of reducing BASE-Fire's overestimation of burned area during peak fire seasons

317 (Figure 5b, Figure S3), although we note that DNN-Fire-OBS is biased high during low fire

318 seasons (March and April).

319
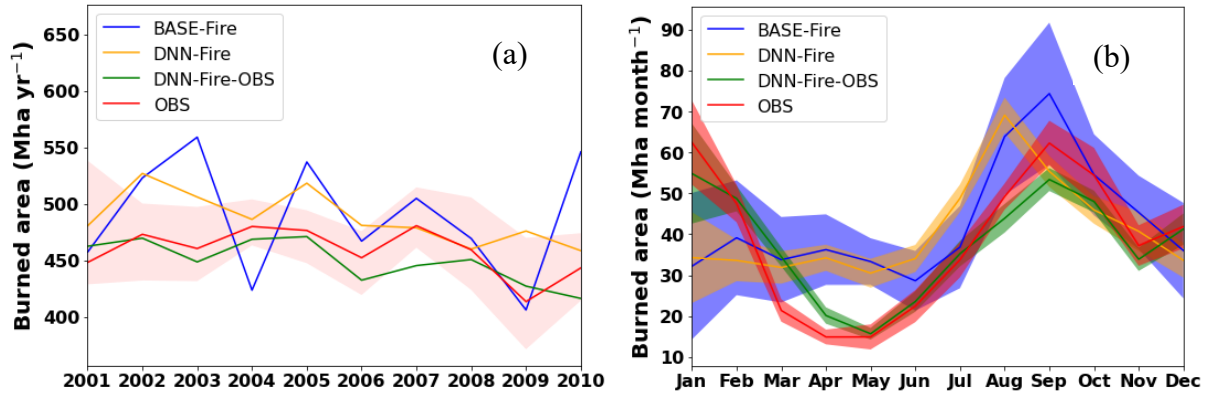
321 **Figure 5**. Inter-annual variation of burned area from years 2001 to 2010 (a) and the averaged

322 seasonal cycle (b) of burned area estimated by the ELMv1 process-based wildfire model (BASE-

323 Fire), Deep Neural Network wildfire model (DNN-Fire), Deep Neural Network wildfire model

324 fine-tuned with observations (DNN-Fire-OBS), and observations.

325

326 **3.3 Prognostic simulation and limitations**

327 We next evaluated the DNN-Fire-OBS model against observations for the period 2011 to

328 2015, using data which were not used to train and validate the model. Overall, DNN-Fire-OBS

329 simulated 469-514 Mha yr^{-1} global burned area, compared with observations 349-509 Mha yr^{-1}.

330 Note that the large observational ranges were mainly due to the differences among the five

331 burned area products rather than the inter-annual variability (Figure 6). Regionally, DNN-Fire-

332 OBS overestimated NHAF, SHAF and SHSA annual burned area by 8, 6, 2 Mha yr^{-1},

333 respectively (Figure 6) compared with the observational mean. Averaged latitudinal distribution

334 of simulated burned area during this period showed that global wildfire activity peaked around

335 S10°- S15° and N5°-N10°, together accounting for burning 12-16% of the land surface (Figure

336 7). These two peaks were dominated by large burned area over Southern (SHAF) and Northern

337 Hemisphere Africa (NHAF) fire regions. Compared with observations, DNN-Fire-OBS

338 simulated reasonable burned area latitudinal distributions (Figure 7). We also compared the nine

339   FireMIP models [*Rabin et al.*, 2017; *Teckentrup et al.*, 2018] and found diverse latitudinal

340   distribution of burned area. The across model differences were much larger than the inter-annual

341   variation simulated by each individual model, which indicated large model structural

342   uncertainties. Validation was also conducted for the historical period 1981-2000, when most of

343   the satellite based burned area data were not available. Compared with charcoal index inferred

344   burned area during 1981-2000 (Figure S4), DNN-Fire-OBS model reasonably captured the

345   declining of burned area from ~530 Mha yr^{-1} to 490 Mha yr^{-1}. In summary, DNN-Fire-OBS

346   simulation is reasonably accurate and: (1) improved the simulated wildfire spatial and temporal

347   distributions in ELMv1; (2) enabled effective and efficient parameterization of fires at regional

348   scale.

349
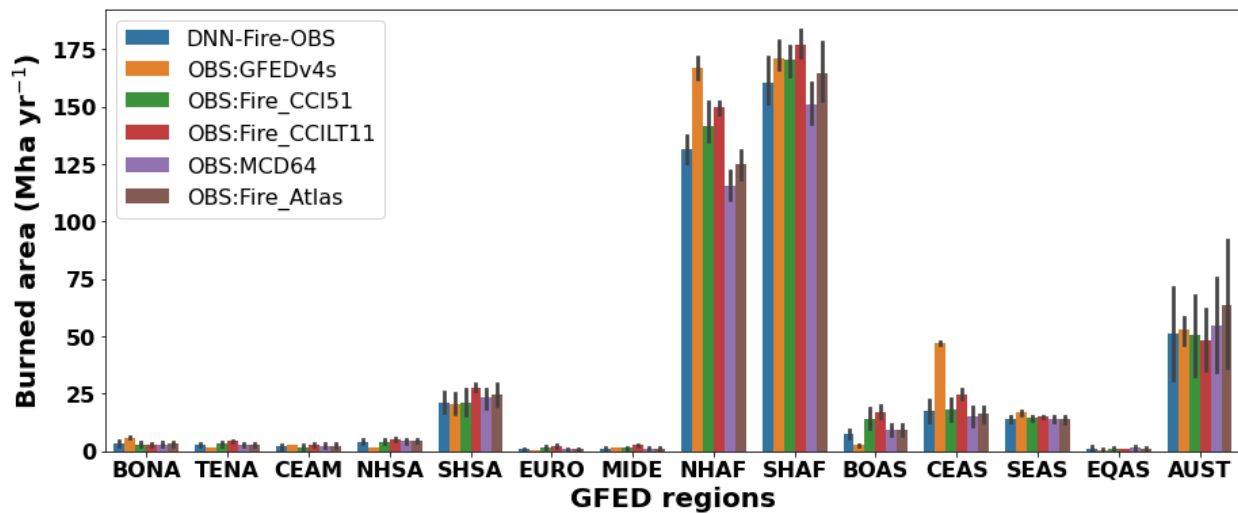
350

351   **Figure 6.** Prognostic simulation of annual wildfire burned area with the Deep Neural Network

352   wildfire model fine-tuned with observations (DNN-Fire-OBS) compared with five burned area

353   products (Table S1) over 2011-2015 for 14 GFED regions.

354
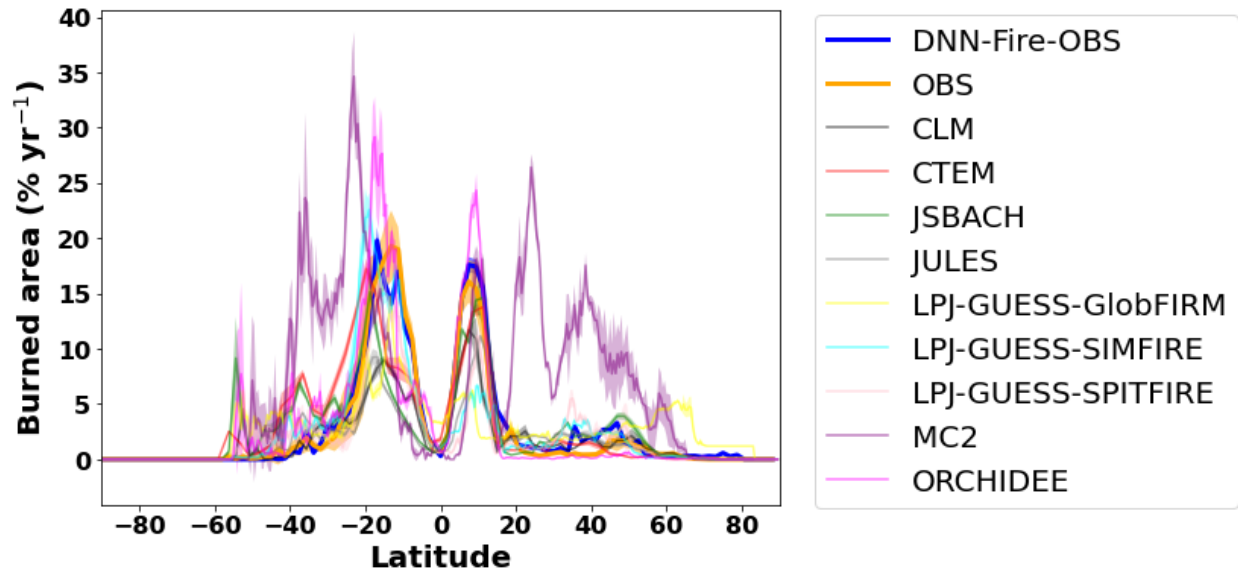
355

356 **Figure 7.** Prognostic simulation of wildfire burned area (2011-2015) with the Deep Neural

357 Network wildfire model fine-tuned with observations (DNN-Fire-OBS) compared with

358 observations and nine FireMIP models outputs.

359

360   This study focuses on design, development, and parameterization of the DNN fire model

361 within the E3SM model interface. In this way the DNN model can be readily coupled in the

362 future and iteratively simulate climate, ecosystem fuel conditions, and fire dynamics. Although

363 no feedbacks exist between biomass/tree cover and burned area were allowed under current

364 offline mode, this study is an important step towards fully coupling E3SM and the DNN-Fire

365 models in the future. We acknowledge several challenges and limitations in our modeling

366 framework. First, the DNN model uncertainty was subject to the accuracy of climate forcings as

367 well as other physical driving variables simulated by the physical wildfire model (ELMv1). For

368 example, in this work ELM simulation of soil temperature, soil moisture, fuel load and so on is

369 subject to the uncertainty of GSWP3 forcings. Furthermore, those simulated variables served as

370 inputs for the DNN model and would result in burned area prediction uncertainty. It was

371 challenging to eliminate the forcing uncertainties in this work, but we could at least evaluate the

372 magnitude of these uncertainties. We ran the DNN-Fire-OBS model with alternative forcings of

373 CRU-JRA, NCEP-DOE2, and CDAS soil moisture from 2001 to 2010 and compared the results

374 with DNN-Fire-OBS driven by default inputs (Figure S5). The results showed relatively larger

375 uncertainties from climate forcing than that from soil moisture forcing particularly over the

376   major fire regions (e.g., SHSA, SHAF, and NHAF). For fuel load, although no transient dataset

377   of global living biomass existed yet, we directly compared the ELM model simulated biomass

378   with the global estimate (GEOCARBON ~ 455 Pg C). We found that the modeled present-day

379   biomass continuously increased from 425 to 470 Pg C and compared reasonably well with the

380   global benchmark (Figure S6). Future work will focus on evaluating the uncertainties from dead

381   fuel load and fuel temperature variables.

382   Second, the original ELMv1 wildfire model has a unified mathematical representation of

383   how fuel, climate, and social-economic conditions control wildfire burned area [*F Li et al.*,

384   2012]. However, training one single DNN wildfire model across the globe will produce a model

385   dominated by gridcells that have high burned area (*e.g.*, Africa). The performance of the trained

386   DNN model, therefore, will likely have larger biases over the low fire gridcells although the

387   globally aggregated burned area could be reasonable. We partly overcame this challenge by

388   applying the widely used 14 GFED fire regions that assume unique and relatively uniform

389   dynamics over each region [*Giglio et al.*, 2006b], and employed stratified random sampling

390   method for training and testing datasets. Although the regionally specific wildfire model

391   introduces additional complexity, it better represents distinct characteristics of wildfire activity

392   over different climate regimes and biomes [*Zhu and Zhuang*, 2013; *Zou et al.*, 2019] and allows

393   for future analyses of how the relevant controllers vary across the globe.

394   Thirdly, the cost function and the training of DNN model relied on the normality

395   assumption of burned area data. Therefore, the DNN model error might be dominated by highly

396   burned gridcells. A potential solution is to use *log* transformation on non-normal data or the

397   resultant cost function [*Kelley et al.*, 2021]. Finally, our GFED region-based parameterization

398   strategy relied on the combination of climate and biome types, while an alternative

399   parameterization strategy for DNN-Fire model could be based on plant functional type

400   distributions. Based on our analysis, the PFT-based DNN-Fire model had similar performance

401   compared with the GFED-based model (Figure S7, S8). Since the GFED regions were defined by

402   present-day climate and fire regimes, our GFED-based models may not fully capture the changes

403   of future fire dynamics due to longer-time scale climate and fire regimes changes.

404

405   **4. Conclusions**

In this study, we first surrogated the baseline ELMv1 wildfire model with a Deep Neural Network (DNN) approach (Pearson correlation coefficient = 0.91 (p value < 0.01), R^2 = 0.79). The development was based on inputs and outputs from the baseline ELMv1 wildfire simulation, which is process-based and reasonably simulates global burned area, although regional biases existed. We then calibrated the neural network weights using the years 2001-2010 observationally inferred burned area. The final calibrated DNN wildfire model (DNN-Fire-OBS) was shown to be more accurate over the 14 GFED regions. For example, reductions in absolute error over Africa, South America, and Europe were by ~90%. More importantly, the DNN-Fire-OBS model parameters could be calibrated within minutes, compared with traditional ELMv1 parameterization ensemble simulations that consume a large amount of computational time. The improved DNN-Fire-OBS model also accurately prognosed global and regional burned area in the five-year period following the training period from 2011 to 2015 (modeled 469-514 Mha yr^{-1}). We conclude that the improved surrogate wildfire model (DNN-Fire-OBS) developed in this study can serve as an effective alternative to the process-based fire model currently used in ELMv1. More broadly, we conclude that machine learning techniques can facilitate earth system model development, parameterization, and uncertainty reduction with high efficiency and accuracy.

Acknowledgements

This research was supported by Energy Exascale Earth System Modeling (E3SM, https://e3sm.org/) Project and the Reducing Uncertainties in Biogeochemical Interactions through Synthesis and Computation (RUBISCO) Scientific Focus Area, Office of Biological and Environmental Research of the U.S. Department of Energy Office of Science. Lawrence Berkeley National Laboratory (LBNL) is managed by the University of California for the U.S. Department of Energy under contract DE-AC02-05CH11231.

Author contribution

Q.Z., W.J.R, designed the study, Q.Z., W.J.R, L.X.., and J.T.R designed model experiments, Q.Z. and F.L. wrote code and run experiments, L.Z, K.Y, H.W., J.G all contribute to the results interpretation, and writing.

Code availability

https://zenodo.org/record/5508795#.YUGjg55KiDU

Data availability

GFEDv4s: https://daac.ornl.gov/VEGETATION/guides/fire_emissions_v4.html

Fire_CCI51: https://geogra.uah.es/fire_cci/firecci51.php

Fire_CCILT11: https://geogra.uah.es/fire_cci/fireccilt11.php

MCD64: https://modis-fire.umd.edu/files/MODIS_C6_Fire_User_Guide_C.pdf

Fire_Atlas: https://www.globalfiredata.org/fireatlas.html

FireMIP model outputs: https://zenodo.org/record/3555562/accessrequest

Reference

Abatzoglou, J. T., and A. P. Williams (2016), Impact of anthropogenic climate change on wildfire across western US forests, *Proceedings of the National Academy of Sciences*, *113*(42), 11770-11775.

Andela, N., D. Morton, L. Giglio, Y. Chen, G. Van Der Werf, P. Kasibhatla, R. DeFries, G. Collatz, S. Hantson, and S. Kloster (2017), A human-driven decline in global burned area, *Science*, *356*(6345), 1356-1362.

Andela, N., D. C. Morton, L. Giglio, R. Paugam, Y. Chen, S. Hantson, G. R. Van Der Werf, and J. T. Randerson (2019), The Global Fire Atlas of individual fire size, duration, speed and direction, *Earth System Science Data*, *11*(2), 529-552.

Arora, V. K., and G. J. Boer (2005), Fire as an interactive component of dynamic vegetation models, *Journal of Geophysical Research: Biogeosciences*, *110*(G2).

Bond, W. J., F. I. Woodward, and G. F. Midgley (2005), The global distribution of ecosystems in a world without fire, *New phytologist*, *165*(2), 525-538.

Bond-Lamberty, B., S. D. Peckham, D. E. Ahl, and S. T. Gower (2007), Fire as the dominant driver of central Canadian boreal forest carbon balance, *Nature*, *450*(7166), 89-92.

Bowd, E. J., S. C. Banks, C. L. Strong, and D. B. Lindenmayer (2019), Long-term impacts of wildfire and logging on forest soils, *Nature Geoscience*, *12*(2), 113-118.

Brando, P., B. Soares-Filho, L. Rodrigues, A. Assunção, D. Morton, D. Tuchschneider, E. Fernandes, M. Macedo, U. Oliveira, and M. Coe (2020), The gathering firestorm in southern Amazonia, *Science advances*, *6*(2), eaay1632.

Cecil, D. J., D. E. Buechler, and R. J. Blakeslee (2014), Gridded lightning climatology from TRMM-LIS and OTD: Dataset description, *Atmospheric Research*, *135*, 404-414.

Chambers, S., and F. Chapin (2002), Fire effects on surface-atmosphere energy exchange in Alaskan black spruce ecosystems: Implications for feedbacks to regional climate, *Journal of Geophysical Research: Atmospheres*, *107*(D1), FFR 1-1-FFR 1-17.

Chen, Y., J. T. Randerson, S. R. Coffield, E. Foufoula-Georgiou, P. Smyth, C. A. Graff, D. C. Morton, N. Andela, G. R. van der Werf, and L. Giglio (2020), Forecasting global fire emissions on

476 subseasonal to seasonal (S2S) time scales, *Journal of advances in modeling earth systems*, *12*(9),
477 e2019MS001955.
478 Chen, Y., J. T. Randerson, D. C. Morton, R. S. DeFries, G. J. Collatz, P. S. Kasibhatla, L. Giglio, Y.
479 Jin, and M. E. Marlier (2011), Forecasting fire season severity in South America using sea
480 surface temperature anomalies, *Science*, *334*(6057), 787-791.
481 Clark, T. L., J. Coen, and D. Latham (2004), Description of a coupled atmosphere–fire model,
482 *International Journal of Wildland Fire*, *13*(1), 49-63.
483 Coffield, S. R., C. A. Graff, Y. Chen, P. Smyth, E. Foufoula-Georgiou, and J. T. Randerson (2019),
484 Machine learning to predict final fire size at the time of ignition, *International journal of*
485 *wildland fire*.
486 Day, C. (2004), Smoke from burning vegetation changes the coverage and behavior of clouds,
487 *PhT*, *57*(5), 24-24.
488 Dirmeyer, P. A., X. Gao, M. Zhao, Z. Guo, T. Oki, and N. Hanasaki (2006), GSWP-2: Multimodel
489 analysis and implications for our perception of the land surface, *Bulletin of the American*
490 *Meteorological Society*, *87*(10), 1381-1398.
491 Dobson, J. E., E. A. Bright, P. R. Coleman, R. C. Durfee, and B. A. Worley (2000), LandScan: a
492 global population database for estimating populations at risk, *Photogrammetric engineering*
493 *and remote sensing*, *66*(7), 849-857.
494 Finney, M. A. (1998), *FARSITE, Fire Area Simulator--model development and evaluation*, US
495 Department of Agriculture, Forest Service, Rocky Mountain Research Station.
496 French, N. H., M. A. Whitley, and L. K. Jenkins (2016), Fire disturbance effects on land surface
497 albedo in Alaskan tundra, *Journal of Geophysical Research: Biogeosciences*, *121*(3), 841-854.
498 Ganapathi Subramanian, S., and M. Crowley (2018), Using spatial reinforcement learning to
499 build forest wildfire dynamics models from satellite images, *Frontiers in ICT*, *5*, 6.
500 Giglio, L., L. Boschetti, D. P. Roy, M. L. Humber, and C. O. Justice (2018), The Collection 6 MODIS
501 burned area mapping algorithm and product, *Remote sensing of environment*, *217*, 72-85.
502 Giglio, L., I. Csiszar, and C. O. Justice (2006a), Global distribution and seasonality of active fires
503 as observed with the Terra and Aqua Moderate Resolution Imaging Spectroradiometer (MODIS)
504 sensors, *Journal of geophysical research: Biogeosciences*, *111*(G2).
505 Giglio, L., J. T. Randerson, and G. R. Van Der Werf (2013), Analysis of daily, monthly, and annual
506 burned area using the fourth-generation global fire emissions database (GFED4), *Journal of*
507 *Geophysical Research: Biogeosciences*, *118*(1), 317-328.
508 Giglio, L., G. Van der Werf, J. Randerson, G. Collatz, and P. Kasibhatla (2006b), Global estimation
509 of burned area using MODIS active fire observations.
510 Girardin, M. P., and M. Mudelsee (2008), Past and future changes in Canadian boreal wildfire
511 activity, *Ecological Applications*, *18*(2), 391-406.
512 Goodfellow, I., Y. Bengio, and A. Courville (2016), *Deep learning*, MIT press Cambridge.
513 Goss, M., D. L. Swain, J. T. Abatzoglou, A. Sarhadi, C. A. Kolden, A. P. Williams, and N. S.
514 Diffenbaugh (2020), Climate change is increasing the likelihood of extreme autumn wildfire
515 conditions across California, *Environmental Research Letters*, *15*(9), 094016.
516 Hantson, S., A. Arneth, S. P. Harrison, D. I. Kelley, I. C. Prentice, S. S. Rabin, and S. Archibald
517 (2016), The status and challenge of global fire modelling, *Biogeosciences*, *13*, 3359-3375.

518 Harden, J. W., K. L. Manies, M. R. Turetsky, and J. C. Neff (2006), Effects of wildfire and
519 permafrost on soil organic matter and soil climate in interior Alaska, *Global Change Biology*,
520 *12*(12), 2391-2403.
521 Heyerdahl, E. K., L. B. Brubaker, and J. K. Agee (2002), Annual and decadal climate forcing of
522 historical fire regimes in the interior Pacific Northwest, USA, *The Holocene*, *12*(5), 597-604.
523 Holden, Z. A., A. Swanson, C. H. Luce, W. M. Jolly, M. Maneta, J. W. Oyler, D. A. Warren, R.
524 Parsons, and D. Affleck (2018), Decreasing fire season precipitation increased recent western
525 US forest wildfire activity, *Proceedings of the National Academy of Sciences*, *115*(36), E8349-
526 E8357.
527 Hurtt, G. C., L. Chini, R. Sahajpal, S. Frolking, B. L. Bodirsky, K. Calvin, J. C. Doelman, J. Fisk, S.
528 Fujimori, and K. K. Goldewijk (2020), Harmonization of global land-use change and management
529 for the period 850–2100 (LUH2) for CMIP6, *Geoscientific Model Development Discussions*, 1-65.
530 Jiang, Y., X.-Q. Yang, X. Liu, Y. Qian, K. Zhang, M. Wang, F. Li, Y. Wang, and Z. Lu (2020), Impacts
531 of wildfire aerosols on global energy budget and climate: The role of climate feedbacks, *Journal*
532 *of Climate*, *33*(8), 3351-3366.
533 Kasischke, E. S., and L. P. Bruhwiler (2002), Emissions of carbon dioxide, carbon monoxide, and
534 methane from boreal forest fires in 1998, *Journal of Geophysical Research: Atmospheres*,
535 *107*(D1), FFR 2-1-FFR 2-14.
536 Keeley, J. E., and A. D. Syphard (2018), Historical patterns of wildfire ignition sources in
537 California ecosystems, *International journal of wildland fire*, *27*(12), 781-799.
538 Kelley, D. I., I. Bistinas, R. Whitley, C. Burton, T. R. Marthews, and N. Dong (2019), How
539 contemporary bioclimatic and human controls change global fire regimes, *Nature Climate*
540 *Change*, *9*(9), 690-696.
541 Kelley, D. I., B. Chantelle, H. Chris, M. A. Brown, W. Rhys, and D. Ning (2021), Low
542 meteorological influence found in 2019 Amazonia fires, *Biogeosciences*, *18*, 787-804.
543 Kingma, D. P., and J. Ba (2014), Adam: A method for stochastic optimization, *arXiv preprint*
544 *arXiv:1412.6980*.
545 Knorr, W., T. Kaminski, A. Arneth, and U. Weber (2014), Impact of human population density on
546 fire frequency at the global scale, *Biogeosciences*, *11*(4), 1085-1102.
547 Koven, C. D., W. J. Riley, Z. M. Subin, J. Y. Tang, M. S. Torn, W. D. Collins, G. B. Bonan, D. M.
548 Lawrence, and S. C. Swenson (2013), The effect of vertically resolved soil biogeochemistry and
549 alternate soil C and N models on C dynamics of CLM4, *Biogeosciences*, *10*, 7109-7131.
550 Lamarque, J. F., J. T. Kiehl, G. P. Brasseur, T. Butler, P. Cameron‑Smith, W. D. Collins, W. J.
551 Collins, C. Granier, D. Hauglustaine, and P. G. Hess (2005), Assessing future nitrogen deposition
552 and carbon cycle feedback using a multimodel approach: Analysis of nitrogen deposition,
553 *Journal of Geophysical Research: Atmospheres*, *110*(D19).
554 Lenihan, J. M., and D. Bachelet (2015), Historical climate and suppression effects on simulated
555 fire and carbon dynamics in the conterminous United States, *Global Vegetation Dynamics:*
556 *Concepts and Applications in the MC1 Model, edited by: Bachelet, D. and Turner, D., AGU*
557 *Geophysical Monographs*, *214*, 17-30.
558 Li, F., M. Val Martin, M. O. Andreae, A. Arneth, S. Hantson, J. W. Kaiser, G. Lasslop, C. Yue, D.
559 Bachelet, and M. Forrest (2019), Historical (1700–2012) global multi-model estimates of the fire
560 emissions from the Fire Modeling Intercomparison Project (FireMIP), *Atmospheric Chemistry*
561 *and Physics*, *19*(19), 12545-12567.

562 Li, F., X. Zeng, and S. Levis (2012), A process-based fire parameterization of intermediate
563 complexity in a Dynamic Global Vegetation Model, *Biogeosciences*, *9*(7).

564 Lizundia-Loiola, J., G. Otón, R. Ramo, and E. Chuvieco (2020), A spatio-temporal active-fire
565 clustering approach for global burned area mapping at 250 m from MODIS data, *Remote
566 Sensing of Environment*, *236*, 111493.

567 Lizundia-Loiola, J., M. Pettinari, E. Chuvieco, T. Storm, and J. Gómez-Dans (2018), ESA CCI ECV
568 Fire Disturbance: Algorithm Theoretical Basis Document-MODIS, version 2.0, edited,
569 Fire_cci_D2.

570 Mahowald, N., T. D. Jickells, A. R. Baker, P. Artaxo, C. R. Benitez‑Nelson, G. Bergametti, T. C.
571 Bond, Y. Chen, D. D. Cohen, and B. Herut (2008), Global distribution of atmospheric phosphorus
572 sources, concentrations and deposition rates, and anthropogenic impacts, *Global
573 Biogeochemical Cycles*, *22*(4).

574 Mekonnen, Z. A., W. J. Riley, J. T. Randerson, R. F. Grant, and B. M. Rogers (2019), Expansion of
575 high-latitude deciduous forests driven by interactions between climate warming and fire,
576 *Nature plants*, *5*(9), 952-958.

577 Oliver, A. K., M. A. Callaham Jr, and A. Jumpponen (2015), Soil fungal communities respond
578 compositionally to recurring frequent prescribed burning in a managed southeastern US forest
579 ecosystem, *Forest Ecology and Management*, *345*, 1-9.

580 Papakosta, P., G. Xanthopoulos, and D. Straub (2017), Probabilistic prediction of wildfire
581 economic losses to housing in Cyprus using Bayesian network analysis, *International journal of
582 wildland fire*, *26*(1), 10-23.

583 Pellegrini, A. F., A. Ahlström, S. E. Hobbie, P. B. Reich, L. P. Nieradzik, A. C. Staver, B. C.
584 Scharenbroch, A. Jumpponen, W. R. Anderegg, and J. T. Randerson (2018), Fire frequency drives
585 decadal changes in soil carbon and nitrogen and ecosystem productivity, *Nature*, *553*(7687),
586 194-198.

587 Pellegrini, A. F., S. E. Hobbie, P. B. Reich, A. Jumpponen, E. J. Brookshire, A. C. Caprio, C.
588 Coetsee, and R. B. Jackson (2020), Repeated fire shifts carbon and nitrogen cycling by changing
589 plant inputs and soil decomposition across ecosystems, *Ecological Monographs*, e01409.

590 Preisler, H. K., and A. L. Westerling (2007), Statistical model for forecasting monthly large
591 wildfire events in western United States, *Journal of Applied Meteorology and Climatology*,
592 *46*(7), 1020-1030.

593 Prentice, S., and D. Mackerras (1977), The ratio of cloud to cloud-ground lightning flashes in
594 thunderstorms, *Journal of Applied Meteorology*, *16*(5), 545-550.

595 Rabin, S. S., J. R. Melton, G. Lasslop, D. Bachelet, M. Forrest, S. Hantson, J. O. Kaplan, F. Li, S.
596 Mangeon, and D. S. Ward (2017), The Fire Modeling Intercomparison Project (FireMIP), phase
597 1: experimental and analytical protocols with detailed model descriptions, *Geoscientific Model
598 Development*, *10*(3), 1175-1197.

599 Radke, D., A. Hessler, and D. Ellsworth (2019), FireCast: Leveraging Deep Learning to Predict
600 Wildfire Spread, paper presented at IJCAI.

601 Randerson, J. T., H. Liu, M. G. Flanner, S. D. Chambers, Y. Jin, P. G. Hess, G. Pfister, M. Mack, K.
602 Treseder, and L. Welp (2006), The impact of boreal forest fire on climate warming, *science*,
603 *314*(5802), 1130-1132.

604 Riley, K., and M. Thompson (2017), An uncertainty analysis of wildfire modeling, *Natural hazard
605 uncertainty assessment: modeling and decision support. Monograph*, *223*, 193-213.

606   Ross, A. N., M. J. Wooster, H. Boesch, and R. Parker (2013), First satellite measurements of
607   carbon dioxide and methane emission ratios in wildfire plumes, *Geophysical Research Letters*,
608   *40*(15), 4098-4102.
609   Rother, D., and F. De Sales (2020), Impact of Wildfire on the Surface Energy Balance in Six
610   California Case Studies, *Boundary-Layer Meteorology*, 1-24.
611   Rothermel, R. C. (1972), A mathematical model for predicting fire spread in wildland fuels,
612   *Intermountain Forest & Range Experiment Station, Forest Service, US Department of*
613   *Agriculture*, *115*.
614   Saha, M. V., T. M. Scanlon, and P. D'Odorico (2019), Climate seasonality as an essential
615   predictor of global fire activity, *Global Ecology and Biogeography*, *28*(2), 198-210.
616   Sayad, Y. O., H. Mousannif, and H. Al Moatassime (2019), Predictive modeling of wildfires: A
617   new dataset and machine learning approach, *Fire safety journal*, *104*, 130-146.
618   Schmidhuber, J. (2015), Deep learning in neural networks: An overview, *Neural networks*, *61*,
619   85-117.
620   Stephenson, C., J. Handmer, and R. Betts (2013), Estimating the economic, social and
621   environmental impacts of wildfires in Australia, *Environmental Hazards*, *12*(2), 93-111.
622   Syphard, A. D., V. C. Radeloff, J. E. Keeley, T. J. Hawbaker, M. K. Clayton, S. I. Stewart, and R. B.
623   Hammer (2007), Human influence on California fire regimes, *Ecological applications*, *17*(5),
624   1388-1402.
625   Teckentrup, L., G. Lasslop, D. Bachelet, M. Forrest, S. Hantson, F. Li, J. R. Melton, C. Yue, A.
626   Arneth, and S. P. Harrison (2018), Simulations of historical burned area: A comparison of global
627   fire models in FireMIP, *EGUGA*, 17537.
628   Thonicke, K., A. Spessa, I. Prentice, S. P. Harrison, L. Dong, and C. Carmona-Moreno (2010), The
629   influence of vegetation, fire spread and fire behaviour on biomass burning and trace gas
630   emissions: results from a process-based model, *Biogeosciences*, *7*(6), 1991-2011.
631   Tonini, M., M. D'Andrea, G. Biondi, S. Degli Esposti, A. Trucchia, and P. Fiorucci (2020), A
632   Machine Learning-Based Approach for Wildfire Susceptibility Mapping. The Case Study of the
633   Liguria Region in Italy, *Geosciences*, *10*(3), 105.
634   Van Der Werf, G. R., J. T. Randerson, L. Giglio, T. T. Van Leeuwen, Y. Chen, B. M. Rogers, M. Mu,
635   M. J. Van Marle, D. C. Morton, and G. J. Collatz (2017), Global fire emissions estimates during
636   1997-2016, *Earth System Science Data*, *9*(2), 697-720.
637   van Vuuren, D. P., P. L. Lucas, and H. Hilderink (2007), Downscaling drivers of global
638   environmental change: Enabling use of global SRES scenarios at the national and grid levels,
639   *Global environmental change*, *17*(1), 114-130.
640   Venevsky, S., K. Thonicke, S. Sitch, and W. Cramer (2002), Simulating fire regimes in human-
641   dominated ecosystems: Iberian Peninsula case study, *Global Change Biology*, *8*(10), 984-998.
642   Walker, X. J., J. L. Baltzer, S. G. Cumming, N. J. Day, C. Ebert, S. Goetz, J. F. Johnstone, S. Potter,
643   B. M. Rogers, and E. A. Schuur (2019), Increasing wildfires threaten historic carbon sink of
644   boreal forest soils, *Nature*, *572*(7770), 520-523.
645   Wang, J.-F., A. Stein, B.-B. Gao, and Y. Ge (2012), A review of spatial sampling, *Spatial Statistics*,
646   *2*, 1-14.
647   Westerling, A. L., H. G. Hidalgo, D. R. Cayan, and T. W. Swetnam (2006), Warming and earlier
648   spring increase western US forest wildfire activity, *science*, *313*(5789), 940-943.

Williams, A. P., J. T. Abatzoglou, A. Gershunov, J. Guzman‑Morales, D. A. Bishop, J. K. Balch, and D. P. Lettenmaier (2019), Observed impacts of anthropogenic climate change on wildfire in California, *Earth's Future*, *7*(8), 892-910.

Xu, L., Z. Qing, J. R. William, C. Yang, W. Hailong, M. Po-Lun, and T. R. James (2021), The influence of fire aerosols on surface climate and gross primary production in the Energy Exascale Earth System Model (E3SM), *Journal of Climate 34*, 7219-7238.

Xu, X., G. Jia, X. Zhang, W. J. Riley, and Y. Xue (2020), Climate regime shift and forest loss amplify fire in Amazonian forests, *Global Change Biology*, *26*(10), 5874-5885.

Yu, Y., J. Mao, P. E. Thornton, M. Notaro, S. D. Wullschleger, X. Shi, F. M. Hoffman, and Y. Wang (2020), Quantifying the drivers and predictability of seasonal changes in African fire, *Nature Communications*, *11*(1), 1-8.

Yue, X., L. J. Mickley, J. A. Logan, and J. O. Kaplan (2013), Ensemble projections of wildfire activity and carbonaceous aerosol concentrations over the western United States in the mid-21st century, *Atmospheric Environment*, *77*, 767-780.

Zheng, H., Z. Yang, W. Liu, J. Liang, and Y. Li (2015), Improving deep neural networks using softplus units, paper presented at 2015 International Joint Conference on Neural Networks (IJCNN), IEEE.

Zhu, Q., and W. J. Riley (2015), Improved modelling of soil nitrogen losses, *Nature Climate Change*, *5*(8), 705-706.

Zhu, Q., W. J. Riley, C. M. Iversen, and J. Kattge (2020), Assessing impacts of plant stoichiometric traits on terrestrial ecosystem carbon accumulation using the E3SM land model, *Journal of Advances in Modeling Earth Systems*, *12*(4), e2019MS001841.

Zhu, Q., W. J. Riley, J. Tang, N. Collier, F. M. Hoffman, X. Yang, and G. Bisht (2019), Representing nitrogen, phosphorus, and carbon interactions in the E3SM Land Model: Development and global benchmarking, *Journal of Advances in Modeling Earth Systems*, doi: 10.1029/2018MS001571.

Zhu, Q., W. J. Riley, J. Tang, and C. D. Koven (2016), Multiple soil nutrient competition between plants, microbes, and mineral surfaces: model development, parameterization, and example applications in several tropical forests, *Biogeosciences*, *13*, 341-363, doi:10.5194/bgd-12-4057-2015.

Zhu, Q., and Q. Zhuang (2013), Improving the quantification of terrestrial ecosystem carbon dynamics over the United States using an adjoint method, *Ecosphere*, *4*(10), doi: dx.doi.org/10.1890/ES1813-00058.00051.

Zhu, Q., and Q. Zhuang (2014), Parameterization and sensitivity analysis of a process‑based terrestrial ecosystem model using adjoint method, *Journal of Advances in Modeling Earth Systems*, *6*(2), 315-331.

Zou, Y., Y. Wang, Z. Ke, H. Tian, J. Yang, and Y. Liu (2019), Development of a REgion‑specific ecosystem feedback fire (RESFire) model in the Community Earth System Model, *Journal of Advances in Modeling Earth Systems*, *11*(2), 417-445.

Zou, Y., Y. Wang, Y. Qian, H. Tian, J. Yang, and E. Alvarado (2020), Using CESM-RESFire to understand climate-fire-ecosystem interactions and the implications for decadal climate variability, *Atmospheric Chemistry and Physics*, *20*(PNNL-SA-150222).